Renewable Pulverized Biomass Fuel for Internal Combustion Engines

Ashraf Elfasakhany [1,*], Mishal Alsehli [1], Bahaa Saleh [1,2], Ayman A. Aly [1,2] and Mohamed Bassuoni [1,3]

[1]   Mechanical Engineering Department, College of Engineering, Taif University, Taif PO Box 888, Saudi Arabia
[2]   Mechanical Engineering Department, Faculty of Engineering, Assiut University, Assiut PO Box 71516, Egypt
[3]   Mechanical Power Engineering Department, Faculty of Engineering, Tanta University, Tanta 31733, Egypt
[*]   Correspondence: ashr12000@yahoo.com or a.taha@tu.edu.sa;
      Tel.: +966-(02)-727-2020; Fax: +966-(02)-727-4299

Abstract: Biomass is currently one of the world's major renewable energy sources. Biomass in a powder form has been recently proposed as the most encouraging of biomass contours, especially because it burns like a gas. In the current study, biomass powder was examined, for the first time, as a direct solid fuel in internal combustion engines. The aim of the current study was to investigate modeling tools for simulation of biomass powder in combustion engines (CE). The biomass powder applied was in a micro-scale size with a typical irregular shape; the powder length was in the range of $75-5800$ μm, and the diameter was in the range $30-1380$ μm. Different mechanisms for biomass powder drying and devolatilization/gasification were proposed, including different schemes' and mechanisms' rate constants. A comparison between the proposed models and experiments was carried out and results showed good matching. Nevertheless, it is important that a biomass powder simulation addresses overlapping/complicated sub-process. During biomass powder combustion, tar was shown to be formed at a rate of 57 wt.%, and, accordingly, the formation and thermal decomposition of tar were modelled in the study, with the results demonstrating that the tar was formed and then disintegrated at temperatures between 700 and 1050 K. Through biomass powder combustion, moisture, tar, and gases were released, mostly from one lateral of particles, which caused ejection of the solid particles. These new phenomena were investigated experimentally and modeled as well. Results also showed that all the proposed models, along with their rate constants, activation energies, and other models' parameters, were capable of reproducing the mass yields of gases, tar, and char at a wide range of working temperatures. The results showed that the gasification/devolatilization model 3 is somewhat simple and economical in the simulation/computation scheme, however, models 1 and 2 are rather computationally heavy and complicated.

Keywords: renewable fuel; biomass powder; micro-scale size; gasification/devolatilization; modeling; validation; combustion engines

1. Introduction

Research into internal combustion engines has in recent years been dedicated to control of pollutant emissions from automobiles [1–3]. Several publications have referred to the high environmental pollutant emissions from automobiles fueled with fossil propulsions [4–8]. One of the possible solutions proposed by researchers was to introduce renewable fuels as an alternative to fossil fuels [9–13]. One of the promising renewable resources is biomass, where it can supply energy for different demands/applications [14–17]. Biomass is reported as one of the largest sources of energy in the world [18]. Biomass, as a solid fuel, could be used in various sizes and shapes; powder biomass

has been recognized as the most attractive form since it burns like gases-fuels [19–22]. Nevertheless, powder biomass combustion is complicated; it comprises overlapping numerous processes, such as drying, gasification/devolatilization, and char formation and oxidation [23]. Among different processes, the gasification and/or devolatilization process is recorded as one of utmost significance and may be one of the most complicated processes [24]. Gasification and/or devolatilization of biomass powder involves a number of chemical reactions in parallel and/or in series leading to the production of a liquid (tar), gases (volatiles), and solid (char). The kinetics of the chemical reactions are determined by applying the Arrhenius equation with different activation energies, reaction orders, and frequency factors. Many researchers have been studying the gasification and/or devolatilization process numerically and experimentally; a review of early research is highlighted subsequently. Sadhukhan et al. [25] studied gasification and/or devolatilization of biomass with coal that is 354–500 μm in size and low heating rate condition, which is not appropriate for the powder biomass in ICEs (Internal combustion engines). Sepman and Goey [26] investigated the experimental rapid gasification and/or devolatilization process of biomass powder at a size of 100 mm. However, the researchers did not provide modeling tools for the process. Kaushal et al. [27] developed a model for fluidized bed biomass at heating rate of less than 1270 K. Hatakeyama and Quinn [28] identified an expression for gasification and/or devolatilization rate of biomass in a large size condition. Haykiri-Acma and Yaman [29] studied the thermal degradation behavior of biomass at low-temperature conditions, such as between 125 and 325 °C. Meesri and Moghtaderi [30] employed gasification and/or devolatilization of biomass using three thermal events with linear kinetics not in flame condition. Nassar [31] presented thermal cracking of biomass during gasification and/or devolatilization using first-order reactions. Vuthaluru [32] applied three thermal reaction pathways to explain the mass loss history of biomass with non-linear reaction kinetics. Sutcu [33] investigated gasification and/or devolatilization behaviors of biomass using a single first-order reaction with varying kinetic parameters in different temperature varieties. Zhou et al. [34] investigated a single first-order reaction kinetic for Chinese biomass. A complete valuable review of studies of biomass gasification and/or devolatilization models was summarized by Di Blasi [35]. Rodrigo et al. [36] presented a computational fluid dynamics (CFD) model for biomass powder in a small-scale boiler combustor. Luz et al. [37] applied experimental and numerical evaluation for pyrolysis of fast powder biomass at laboratory boiler scale. El-Sayed and Mostafa [38] applied thermal gravimetric analysis for kinetic parameter determination and pyrolysis characteristics of biomass fuel powder. Xu et al. [39] applied experimental investigation on flow properties using different biomass powders. Pachón-Morales et al. [40] studied the flow properties of biomass powder under effect of torrefaction intensity. Pachón-Morales et al. [41], in another study, introduced and calibrated the modeling tool of cohesive flow with biomass powder and by using bulk tests. Li et al. [42] investigated mango biomass powder in a bio-electrochemical system at high-performance anode. Medina et al. [43] examined and determined experimentally the minimum explosible concentration of biomass powder. Falk et al. [44] studied the relationship between biomass particle properties and mass flow rate under variability in a screw feeding system. Fang et al. [45] introduced an experimental investigation on the effects of biomass powder properties of the natural downward smoldering. Xie et al. [46] applied experimental analysis on thermal oxidative decomposition and fire characteristics of different straw powders.

In summary, from early models/mechanisms for biomass gasification and/or devolatilization in the literature discussed above and many others, one can outline four issues: (1) a single step global reaction mechanism; (2) a single step with four independent parallel reactions; (3) a single reaction followed by two competed reactions; and (4) three competing reactions to form gas, tar, and char. These models/mechanisms were applied for combustion of large-size biomass particles rather than powder biomass. Accordingly, such mechanisms must be validated and/or tuned for powder fuels to have reasonable rate constants, frequency factors, and activation energies; otherwise, new models dedicated for powder biomass gasification and/or devolatilization should be proposed.

In light of early studies presented above, one may observe that gasification and/or devolatilization of biomass in micro-scale particle size has been rarely introduced [47]. Researchers have reported that the topic requires proposing and investigating mathematical models for such flame conditions [48]. Recently, some gasification and/or devolatilization models have been presented that are similar to those applied in commercial coal in fired working conditions [49]. However, biomass powder in internal combustion engines is typically not examined in the literature. The objective of the current study was to fill this gap and examine biomass powder as a direct fuel injected into internal combustion engines, such as in combustion working conditions, as well as proposing and investigating modeling tools for such powder flame. The powder flame includes different processes, such as particle tracing, drying, devolatilization, gases, tar and char formation, and oxidations. Such processes are complicated and mostly overlap, and, accordingly, the modeling tools should be divided into a couple of stages; in the first stage, which is covered in the current study, drying and devolatilization are modeled and validated. In the second stage, which is covered in a separate study, complete simulation of powder combustion, including the modeling tools in the first stage together with supplementary modeling tools for flame, is investigated. In the first stage, particle tracing in ICE is also covered. The powder biomass motion in engine would be influenced by moisture and/or gases released during drying and/or gasification/devolatilization processes; such an occurrence may also affect the particle cloud and, in turn, biomass powder distribution inside combustion chamber of engine. Subsequently, this effect should be considered for the powder biomass flame in ICEs; however, such influence on particle motion was not considered by researchers, and, in turn, it is covered here.

2. Experimental Data

The experimental data used in the current study was collected from the literature for the fast gasification and/or devolatilization process similar to engine flame conditions. The gasification and/or devolatilization experiments of Nunn et al. [50] were applied in the current research. Such experiments were chosen on the basis of the fact that their heating rate, powder sizes, and flame conditions were similar to our powder biomass flame in the combustion engines; the heating rate was about 1000 K/s and particle sizes were in the range of 48−89 μm. The biomass particles considered in our modeling study were characteristically a non-spherical shape, with sizes in the range of 30−1380 μm in diameter and 75−5800 μm in length. The experiment offered solid mass, tar, char, and gas yields of biomass powder in thermal degradation within temperatures between 400 and 1600 K; for further details about the experimental set up and conditions, please refer to Nunn et al. [50].

3. Mathematical Models and Methods

3.1. Particle Transport Model

In the Eulerian–Lagrangian approach (ELA), the discrete phase biomass powder trajectory is predicted by integrating the force balance on the particle, which was done using the Lagrangian scheme. Such force balance contains particle inertia and other forces acting on the particle motion. The approach considers a shape factor, which is the ratio between the sphere surface area containing same volume as the powder and the powder (non-spherical) surface area. The detailed modeling is descried as follows.

In the current flame condition, the ELA was suitable in being able to simulate the powder/flow motion because the solid phase was in dilute condition, that is, the volume fraction of powder was less than 10^{-3}. The motion of the solid/powder phase is described as

$$\frac{d\left(M_p \vec{U}_p\right)}{dt} = \vec{F}_b + \vec{F}_d + \vec{F}_r \tag{1}$$

where M_p and $\vec{U}_p$ are the mass and velocity of the biomass powder, respectively. In Equation (1), the right hand side is the sum of the most important forces acting on the powder. The body/gravity and drag forces are commonly known as the dominant forces [51]. In addition, one additional force is called rocket force. This force is a result of rapid drying and devolatilization ejected from the solid powder, as discussed and modelled later in the next subsection. First, the body/gravity force is modelled as

$$\vec{F}_b = M_p \vec{g} \tag{2}$$

The drag force powder biomass in non-spherical shape is modelled using drag coefficient, C_d [52,53] as

$$\vec{F}_d = \frac{1}{2} C_d A_{pr} \rho_g \left| \vec{U}_g - \vec{U}_p \right| \left(\vec{U}_g - \vec{U}_p \right) \tag{3}$$

$$C_d = \frac{24}{\mathrm{Re}_p N_1} \left[1 + 0.1118 \left(\mathrm{Re}_p N_1 N_2 \right)^{0.6567} \right] + 0.4305 N_2 / (1 + \frac{3305}{\mathrm{Re}_p N_1 N_2}) \tag{4}$$

where Re_p is the powder Reynolds number, N_1 and N_2 are shape factors, and ψ is the particle sphericity. Such parameters are correlated as

$$\mathrm{Re}_p = \frac{\left| \vec{U}_g - \vec{U}_p \right| \sqrt{D_p L_p}}{\nu_g}, \ N_1 = \left(\frac{1}{3} + \frac{2}{3} \psi^{-0.5} \right)^{-1} \tag{5}$$

$$N_2 = 10^n, n = 1.8148(-\log\psi)^{0.5743} \tag{6}$$

$$\psi = \frac{d_v^2}{d_s^2} = 1.6509 \left(\frac{D_p}{2L_p} \right)^{1/3} \tag{7}$$

$\vec{U}_g$, ν_g, and ρ_g are, respectively, the velocity, kinematic viscosity, and density of gas. A key factor, A_{pr} in Equation (3), called the particle projected area, is modelled as

$$A_{pr} = (1 - a_{pr})\pi D_p^2 / 4 + a_{pr} L_p D_p \tag{8}$$

where a_{pr} is a model constant (varied between 0 and 1, according to powder orientations), $a_{pr} = 1$ represents powder moving with fiber direction parallel to flow field, and $a_{pr} = 0$ represents powder moving with fiber direction normal to flow field. In the current calculation, an average value of $a_{pr} = 0.5$ was applied.

3.2. Modeling of Rocket Propulsion

The physical structure of powder biomass particles is fibrous, as shown in Figure 1, and, in turn, the released moisture/gasses tend to follow the fiber direction rather than being isotropic along the particle surface. In the case of high drying and devolatilization rates (i.e., in flame condition where heating rate of particles is as high as in combustion engines), the particles may be subjected to a propulsion that we refer to as "rocket" force, as the physical process resembles that of rocket propulsion. Accordingly, this may affect particle distribution in the combustion chamber, and, in turn, on flame structure. The effect/phenomenon can be modeled as follows:

$$\frac{d \sum M_{sys} \vec{U}_{sys}}{dt} = \frac{d(m_p \vec{U}_p)}{dt} + \frac{dm_{exit}}{dt} \vec{U}_{exit} \tag{9}$$

Here, $\vec{U}_{sys}$ and M_{sys} represent the velocity and total mass of powder (biomass/char/ash/moisture/volatile); $\vec{U}_p$ and m_p represent the velocity and mass of the solid powder part, Δm_p represents the

change in powder mass due to char oxidation/gasification, and Δm_{exit} represents the mass of volatile and moisture released from the powder at speed $\vec{U}_{exit}$ (see Figure 1).

$$\vec{F}_r = -\frac{dm_{exit}}{dt} \cdot \vec{U}_{exit} \tag{10}$$

$$\frac{dm_{exit}}{dt} = \frac{dm_{vol}}{dt} + \frac{dm_{moist}}{dt} \tag{11}$$

$$\vec{U}_{exit} = \frac{\frac{d}{dt}m_{exit}}{A_{pr}\rho_g}\vec{\tau} \tag{12}$$

$$\vec{F}_r = \frac{\left(\frac{d}{dt}m_{vol} + \frac{d}{dt}m_{mois}\right)^2}{A_{pr}\rho_g}\vec{\tau} \tag{13}$$

$\vec{\tau}$ represents a unit vector along particle fiber direction, for instance, it defines the powder orientation in the flow, as shown in Figure 1.
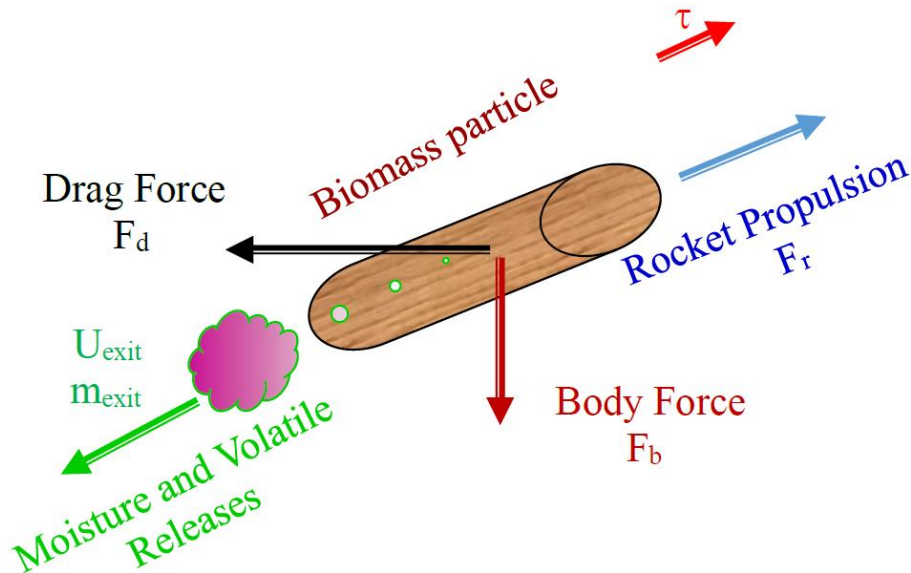

Figure 1. Schematic view of biomass particle and effect forces with moisture and volatile releases from one end and rocket propulsion on the opposite end.

3.3. Particle Heating and Drying Model

Powder biomass combustion contains different steps. Once the powder is introduced into the engine, it is heated up and, in turn, moisture evaporates and leaves the solid powder. After moisture leaves (drying process), or even during late stage of drying, gasification/devolatilization starts and volatiles, tar, and char are produced. In this subsection, the drying model is described, and the devolatilization model is described in the next subsection.

Drying of biomass powder is modelled using a diffusion model. In the model, the moisture release rate from the powder depends on the mass transfer between the powder and the surrounding hot gases [54].

$$\frac{dM_{moist}}{dt} = -h_d A_p (C_{w\infty} - C_{ws}) \tag{14}$$

$$C_{ws} = \frac{P_{sat}}{R_u T_p}, \qquad C_{w\infty} = \rho_g Y_{H2O}, \qquad A_p = \pi D_p L_p \tag{15}$$

$$P_{sat} = 1.1 \times 10^{-5} \exp\left(11 \times (T_p - 273.15)^{0.16}\right) \tag{16}$$

$$h_d = S_h D_g / D_p, \quad S_h = 2 + 0.552 \text{Re}_p^{1/2} Sc^{1/3} \tag{17}$$

Here, C_{ws}, $C_{w\infty}$, Y_{H2O} represent, respectively, the concentration of moisture/steam on the powder surface, concentration of moisture/steam in the gases, and mass fraction of moisture/steam in the gas mixture. Sc is the Schmidt number of the gas mixture (set in the calculation as 0.73); h_d is the mass transfer coefficient; D_g is the diffusion coefficient of the gas mixture; and L_p, D_p, T_p, and A_p are the length, diameter, temperature of the powder, and particle area, respectively.

In the study, another drying model, based on the chemical kinetic model (using Arrhenius expression) [55], was also applied. The numerical simulation showed fairly little difference with the drying model in Equations (14)–(17) because of low moisture content in the powder biomass fuel,

3.4. Gasification/Devolatilization Models

In this study, three gasification and/or devolatilization models for biomass powder were proposed for the first time; a detailed explanation of the models is found in the subsequent sections.

3.4.1. Gasification/Devolatilization Model 1

Model 1 (M1) was proposed based on that the biomass powder would be thermally cracked into char, tar, and gases at different yields; the gases contained lumps of different types, such as CO_2, CO, CH_4, H_2, and H_2O. The five gas types generate in different rates and yields, and, accordingly, different paths for the gas generations were modeled, as shown in Table 1. The tar is divided into two types: *Tar 1* represents heavy tar and *Tar 2* represents light tar, as shown in Table 1. The heavy tar is kept during gasification and/or devolatilization, whereas the light tar is cracked into gases. Further details about the light and heavy tars are discussed later. In Table 1, the last two equations represent the temperature dependence of reaction rates, which is the recognized Arrhenius equations. The rate constants and the hypotheses in the model were adopted in correspondence with the experimental data.

Table 1. Gasification and/or devolatilization model one (M1).

Model	m_i/m_{wood} [%]	A_i (s^{-1})	E_i (kJ/mol)
$wood \xrightarrow{k_i} Char$	15.00	–	–
$wood \xrightarrow{k_i} Tar1$	45.70	1.646×10^6	82.624
$wood \xrightarrow{k_i} Tar2$	10.00	7.411×10^5	99.225
$wood \xrightarrow{k_i} Gas1(CO)$	7.460	2.291×10^3	61.126
$wood \xrightarrow{k_i} Gas2(CO_2)$	10.76	5.888×10^3	59.870
$wood \xrightarrow{k_i} Gas3(CH_4)$	2.800	6.166×10^3	69.499
$wood \xrightarrow{k_i} Gas4(H_2)$	3.140	6.310×10^5	89.176
$wood \xrightarrow{k_i} Gas5(H_2O)$	5.140	2.239×10^3	48.147
$\frac{dm_i}{dt} = k_i m_{wood}$		$k_i = A_i \exp\left(-\frac{E_i}{RT_p}\right)$	

In the table, A_i is frequency factors, E_i is activation energy, m_{wood} is initial wood yield of total mass of particle (wood/char/ash/moisture/volatile), m_i is initial functional group yield, R is universal gas constant, T_p is biomass particle temperature, and *k* is reaction rate.

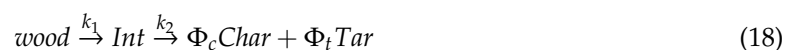### 3.4.2. Gasification/Devolatilization Model 2

Gasification and/or devolatilization model 2 (M2) considered the fact that the powder biomass, in engine combustion working conditions, is cracked into char, tar, and four different gases, as shown in Table 2. The gases are CO, CO_2, H_2O, and unburned hydrocarbons (UHC); the UHC represent all the possible hydrocarbons produced during biomass gasification and/or devolatilization, such as CH_4, C_2H_6, and C_2H_4. The differences between this model (M2) and model 1 (M1) are twofold. Firstly, the tar here is modeled as one module on the basis of the assumption that the light tar (tar 2) would crack very fast into gases, especially with our high heating rate in the combustion engine, and, in turn, the light tar (tar 2) path would be disregarded. Secondary, the gases here contains four modules, in contrast to the five ones in model 1; model 2 assumes that there are many types of gases generated; all such gases are lumped as one overall type, which is denoted as UHC. In Table 2, similar to model 1, the last two equations represent the temperature dependence of reaction rates, which are the recognized Arrhenius equations. The rate constants and the hypotheses in the model are adopted in correspondence to the experimental data.

Table 2. Gasification and/or devolatilization model 2 (M2).

Model	m_i/m_{wood} [%]	A_i (s^{-1})	E_i (kJ/mol)
$wood \overset{k_i}{\rightarrow} Char$	15.00	–	–
$wood \overset{k_i}{\rightarrow} Tar$	55.70	1.646×10^6	82.624
$wood \overset{k_i}{\rightarrow} Gas1\,(CO)$	7.460	2.291×10^3	61.126
$wood \overset{k_i}{\rightarrow} Gas2\,(CO_2)$	10.76	5.888×10^3	59.870
$wood \overset{k_i}{\rightarrow} Gas3\,(UHC)$	0.800	6.166×10^3	69.499
$wood \overset{k_i}{\rightarrow} Gas4\,(H_2O)$	5.140	2.239×10^3	48.147
$\frac{dm_i}{dt} = k_i m_{wood}$	$k_i = A_i \exp\left(-\frac{E_i}{RT_p}\right)$		

3.4.3. Gasification/Devolatilization Model 3

Model 3 (M3) is proposed here according to the fact that the biomass powder could be cracked into an intermediate product (represented as Int in Equation (1)) and then the intermediate is cracked into char and tar using one reaction rate but in two different yields for char and tar. However, the gases are generated in a separate reaction, as shown below. This model assumes that the char and tar are heavy modules, and, in turn, they are generated via one path (in different yields); however, the gases would be generated faster and, in turn, they are in dissimilar pass. Additionally, the gases are lumped into one module. The idea behind model 3 (M3) is in assuming different strategies for the biomass powder gasification/devolatilization compared with models 1 and 2.

$$wood \overset{k_1}{\rightarrow} Int \overset{k_2}{\rightarrow} \Phi_c Char + \Phi_t Tar \tag{18}$$

$$wood \overset{k_3}{\rightarrow} \Phi_g Gas \tag{19}$$

$$\frac{dm_{Int}}{dt} = k_1 m_w, \quad \frac{dm_c}{dt} = k_2 m_{Int}, \quad \frac{dm_t}{dt} = k_2 m_{Int}, \quad \frac{dm_g}{dt} = k_3 m_w \tag{20}$$

$$k_i = A_i \exp\left(-\frac{E_i}{RT_p}\right) \tag{21}$$

$$\begin{aligned}
A_1 &= 2.83 \times 10^{17}\ (s^{-1}) & E_1 &= 242.8\ (kJ/mol) \\
A_2 &= 3.17 \times 10^{14}\ (s^{-1}) & E_2 &= 198.0\ (kJ/mol) \\
A_3 &= 2.32 \times 10^{11}\ (s^{-1}) & E_3 &= 150.7\ (kJ/mol)
\end{aligned} \tag{22}$$

$$\Phi_c = 15\%,\ \Phi_t = 55.7\%,\ \Phi_g = 29.3\% \tag{23}$$

where Int. denotes intermediate product, Φ_g is rate of gases, Φ_t is rate of tar, and Φ_c is rate of char. The rate constants and the hypotheses in the model are adopted in correspondence to the experimental data.

3.5. Tar Gasification and/or Devolatilization Model

During pyrolysis, tar is produced in two main organic layers; the upper layer is called light tar and the lower one is called heavy tar [56]. The light tar contains about 79 compounds, including hydrocarbons (12%), phenol (16.4%), phenolic compounds (27%), acetic acid (3%), and some oxygenate compounds (53%). The heavy tar, on the other hand, contains only about 18 compounds, including lauric acid (6%), phenol (31%), phenolic compound (27%), and some other oxygenate compounds (35%). Due to their different compounds, each tar type (heavy or light) has its diverse properties. The light tar, for example, has a heating value of 10,304 kcal/kg, specific gravity of 0.99, pH 3, and flash point <27 °C. However, the heavy tar has a heating value of 6210 kcal/kg, specific gravity of 1.13, pH 2.5, and flash point of 134 °C [56]. Due to such variances in composition and prosperity, the light tar is easier/faster to burn rather than the heavy tar, and, accordingly, the light tar is cracked partially during the devolatilization process. Referring to the experiment of Nunn et al. [50], as shown afterwards in the results section, the tar outline showed ultimate and then it decreased partially; in order to model such a trend precisely, tar gasification and/or devolatilization sub-processes are applied in the numerical simulations, as shown below, where the kinetic rate is taken from [57,58].

$$\text{Tar} \xrightarrow{k_T} \text{Gas} \tag{24}$$

$$k_T = A_T \exp\left(-\frac{E_T}{RT_g}\right),\ A_T = 4.28 \times 10^6\ 1/s,\ E_T = 107\ \text{kJ/mol} \tag{25}$$

3.6. Biomass Powder Shrinkage Model

The idea behind the shrinkage model is that the solid particle shrinks during the drying and devolatilization processes, as a result of the moisture and volatile leave particles; the shrinkage model provides the varied volume of the solid particle, and it is calculated as follows [59,60]:

$$V_p = V_{gas} + V_{solid} \tag{26}$$

$$V_{gas} = \eta V_{gas}^0 + (1 - \eta)\gamma V_{gas}^0 + \beta(V_{solid}^0 - V_{solid}) \tag{27}$$

$$\frac{V_{solid}}{V_{solid}^0} = \eta + \frac{\alpha M_{char}}{M_{wood}^0} \tag{28}$$

$$\eta = M_{wood}/M_{wood}^0 \tag{29}$$

Here, V_p, V_{gas} and V_{solid} are the complete volume of the particle, and the volume occupied by the moisture/gas and solid in the particle, respectively. V_{gas}^0 and V_{solid}^0 are the initial volumes in the particle occupied by the moisture/gas and the solid in the particle, respectively, which depends on the porosity of the biomass particle (taken as 0.67 here). M_{wood}, M_{wood}^0, and M_{char} are the mass of the biomass particle, the initial mass of the biomass particle, and the mass of char in the particle, respectively. The volume occupied by the solid is assumed to decrease linearly with the particle mass and to increase with char mass [59,60]. In Equations (27) and (28), the model constants are fixed as $\alpha = 0.5$, $\beta = 0$, and $\gamma = 0.5$ [60].

3.7. Simulation Scheme and Methods

An in-house computational fluid dynamics code (CFD) was applied in the current work to simulate the fluid flow in the combustion engine condition. Next, the simulated flow field was applied to calculate the particle motion, which included particle/flow interactions using the Euler-Lagrange approach. Different gasification and/or devolatilization models, in addition to particle projected area, drying, and thermal degradation of powder biomass were combined into the computational fluid dynamics code for the complete simulation of biomass gasification and/or devolatilization. The gas phase transport is described in the current study by the Favre averaged Navier-Stokes equations. In the following section, further details are explained.

In the combustion engines, a premixed mixture of biomass powder and air were injected into the engine combustion chamber through the feeding system via single entry. By igniting the fuel/air mixture, this initiated the combustion process, which is influenced by diffusion of heat and species; the combustion process occurs in four different steps: drying, gasification/devolatilization, volatiles, and char formation and oxidation, yielding solid ash and pollutant gases. The net heat of the biomass powder, solved by a heating balance, appeared as a source/sink of heat in subsequent calculations of the continuous phase energy equation. Similarly, the creation/depletion of species due to biomass powder reactions resulted as source terms in species conservation equations of the gas phase. The Euler-Lagrange approach was applied to solve the two-phase reactive flows. The biomass particle was treated as a dispersed phase and its trajectories were computed in a Lagrangian approach using balance forces on particle motion, as discussed earlier. The gas phase was treated as a continuum by solving equations of mass conservation, species, momentum, and energy. The turbulence model used in the study was the k-ω, which provides a good predicting for reactive flows [36,61]. Due to the presence of solid particles in the flow, the thermal radiation effects were included, and the P1 method was used to solve the radiation model. The WSGG (weighted sum of gray gas) model was applied for solution of the variable absorption coefficient of the gas phase [62].

Computational grid and numerical uncertainties were applied in the study. The numerical uncertainty was mostly due to the approximation between the transport equations and the fixed number of particles inserted into the numerical simulations. Because the finite number of grid points was applied to describe the engine and set number of particle groups that were considered to represent a large number of actual particle size groups, the numerical results showed truncation errors. Such errors can be reduced by using fine grid resolution, a great number of particle size groups, and a great number of injected particles. The numerical uncertainty is insignificant once the numerical results are unresponsive to the changes of particle size groups and grid resolution. On the basis of such a vision, we investigated the grid dependency of results using numerical simulations at several grid resolutions. We found that the grid with $142 \times 30 \times 30$ grid points (in the axis and cross flow directions) was satisfactory in gaining an approximate grid-independent solution. In the cross flow directions, the grid resolution can be low because the existing flow is rather similar to a "plug flow". In the current numerical simulations, 27 size groups were applied to produce smooth and converged drying and gasification/devolatilization source terms for the gas phase transport equations. However, numerical results using more than 27 size groups showed no significant difference compared with the 27 size groups. The particle sizes were interpolated within the biomass powder size range (30−1380 μm for diameter and 75−5800 μm for length). In the simulation, a time step 0.001s was applied, with a total of 5000 time steps used in the averaging calculation. The numerical injection of the particle groups was at 300 parcels per second. Regarding the computational domain and boundary/initial conditions, the simulation was carried out considering a steady state flow process. The inlet boundary conditions specified mixture mass flow rates and system feeding area. The wall was considered to be adiabatic. The mass flow rate at the inlet and the equivalence ratio were set according to the operational parameters, and low equivalence ratio was adopted due to restrictions in the supply system.

4. Results and Discussions

Numerical simulation for biomass powder combustion in internal combustion engines is validated in this section. Firstly, inspiration of rocker propulsion is discussed. Figure 2 shows an image view of the effects of moisture and gases released during gasification/devolatilization of biomass powder flame in the ICEs. As shown, moisture and volatile released from one end of biomass powder, whereas rocket propulsion ejected the particles from the opposite end. Additionally, due to ejection, powders were widely distributed in the combustion chamber of engine. The bright spot in the image demonstrates the burning tail of gases from the particle, whereas the thin short neighborhood represents the hot solid particle. Moreover, in some powders, the released gasses may not have followed the fiber direction and, in turn, rocket propulsion was not recorded, as shown for some powders in Figure 2. In conclusion, this effect/phenomenon is applicable for major biomass powder; besides, the effect/phenomenon is different from one particle to another according to the powder size and heating rate.
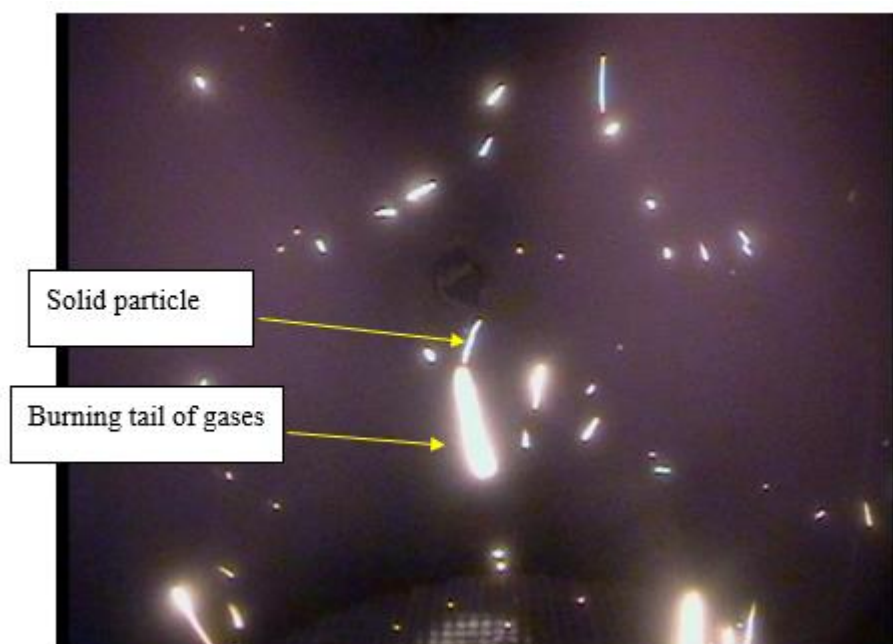

Figure 2. Experimental photo image by high speed camera showing the influence of moisture and volatile releases on the biomass particle motion.

The gasification and/or devolatilization simulation with our three proposed models for biomass powder in combustion engines (flame working conditions) is discussed as follows. The three models/mechanisms along with their rate constants were validated against the devolatilization/gasification experiments of Nunn et al. [50]. The experiment was applied in conditions similar to our fuel biomass flame conditions, as mentioned previously. As shown in Figures 3–5, all the proposed models, along with their rate constants, activation energies, and other model parameters, were capable of reproducing the mass yields of gases, tar, and char at a wide range of working temperatures.
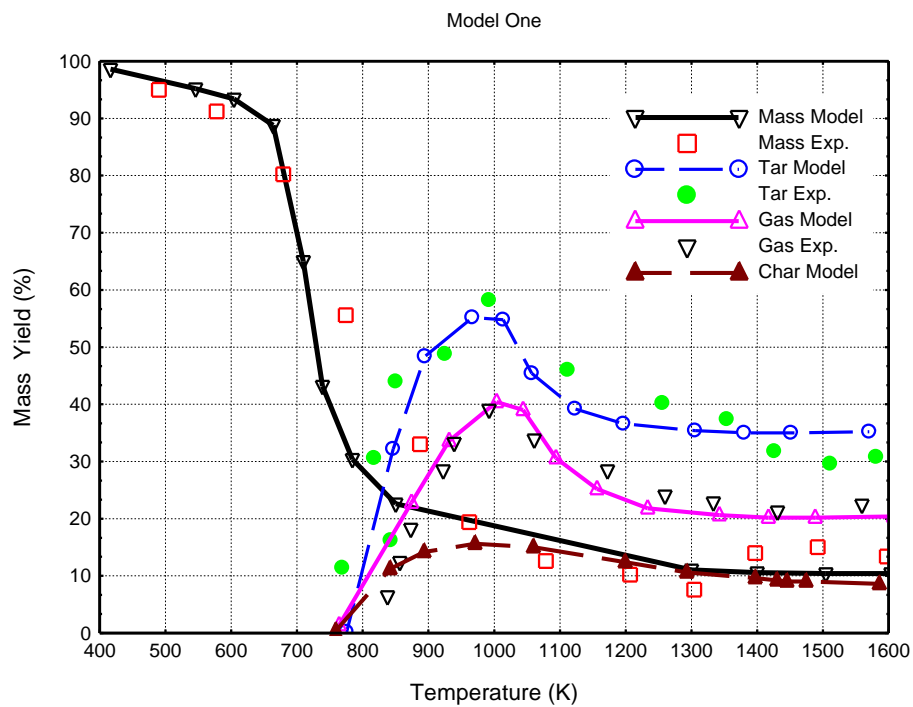
Model One

Figure 3. Simulations of gasification and/or devolatilization model 1 (M1) and experimental measurements (using Nunn et al. [50]) for a mass yield of gases, char, and tar of powder biomass at fast heating rate conditions in combustion engines.
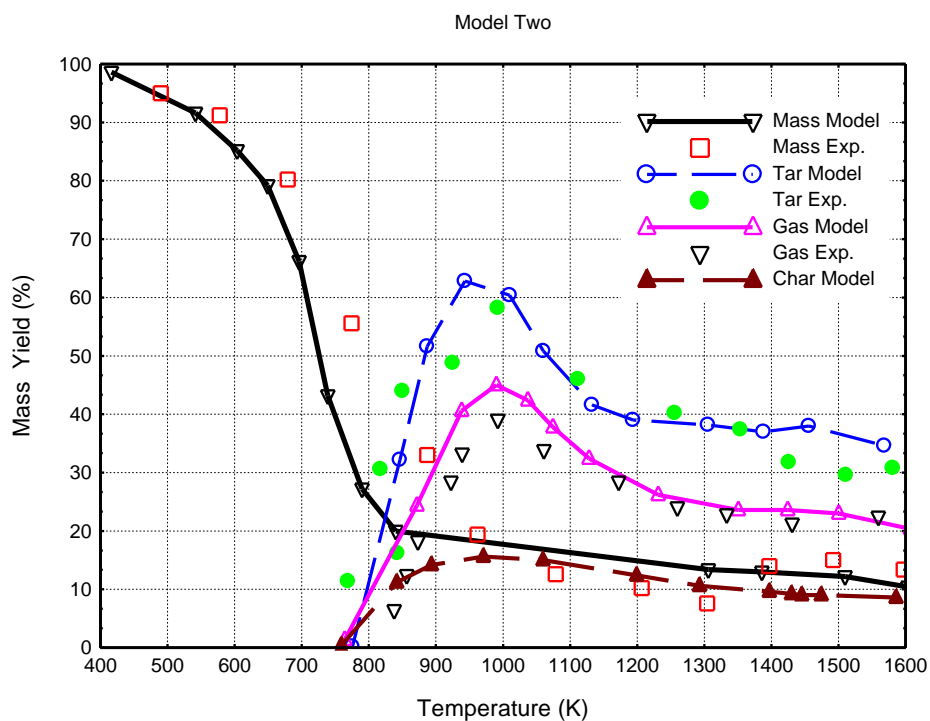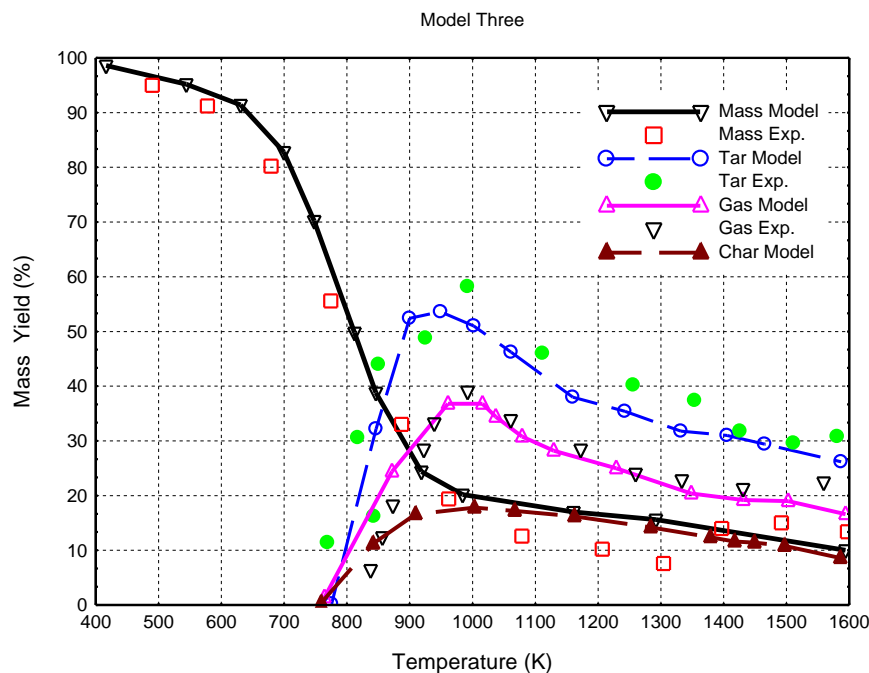
Model Two

Figure 4. Simulations of gasification and/or devolatilization model 2 (M2) and experimental measurements (using Nunn et al. [50]) for a mass yield of gases, char, and tar of powder biomass at fast heating rate conditions in combustion engines.

Figure 5. Simulations of gasification and/or devolatilization model 3 (M3) and experimental measurements (using Nunn et al. [50]) for a mass yield of gases, char, and tar of powder biomass at fast heating rate conditions in combustion engines.

The differences between the proposed three different models/mechanisms are that model 1 and 2 are based on functional group concept; such concept assumes many independent competing reactions to produce solid char, liquid tar, and different gases. Additionally, model 1 represents tar as two components, tar 1 (heavy) and tar 2 (light); in model 2, the generated gases are four different types, however, in model 1 the gases are five types. This is based on the fact that the unburned hydrocarbons in model 2 represent all the light hydrocarbons. Model 3, on the other hand, is based on two competing reaction pathways, one for gas and another for intermediate status; the intermediate product generates tar and char afterward in one reaction pathway.

In the numerical simulation, the tar gasification and/or devolatilization sub-process is applied to model the trend of tar in combustion conditions. As shown in Figures 3–5, tar is started to be formed at a temperature of 700 K; at temperature 850 K, tar showed a peak value (57% weight basis) and then cracked until the temperature reached 1050 K. For temperatures higher than 1050 K, tar and other gasification and/or devolatilization yields (char and gases) were unrelated to engine heating conditions. At low heating conditions (<700 K), the gases, char, and tar yields were somewhat stumpy. It is important to notice that the tar was generated and cracked at the same time; hence, the peak of tar was because of the variance between the rates of depletion and the creation of tar. Specifically, the peak refers to a quicker creation rate than depletion rate. Nevertheless, tar yield decreased with temperature subsequently because of moderate gasification and/or the devolatilization/cracking process of tar, whereas the formation was completed due to complete moss loss of solid biomass. The cracked tar was mainly for the light type, but the heavy type remained. This was the idea behind proposing the gasification and/or devolatilization model 1, which differentiated between a couple of tar products as heavy and light types, as shown in Table 1. In order to simulate the ultimate of the tar trend, subordinate tar reaction was considered in the simulations (see Equations (24)–(25)), whereas the kinetic rate was taken from the early studies [57,58]. Subsequently in the tar model, our proposed models for gasification and/or devolatilization can simulate the tar yield properly, as shown in Figures 3–5.

Analysis of mass loss of biomass powder showed a major tar formation rate by up to 57 wt.%, which was partially cracked to reach 45 wt.%.

From the simulation results, one can be shown that gasification and/or devolatilization M3 was somewhat simple and economical in the simulation/computation period; however, models 1 and 2 were computationally heavy. Additionally, both models 1 and 2 presented much more details for the gases based on function group concept; details of this concept is presented in our early publications [57,63]. The calibration of models 1 and 2 requires more experiments, which are applied from our previous work [63]. Both models showed superior potential because they offered the opportunity for explanation thorough chemical species during the powder gasification and/or devolatilization process of biomass, but were expensive in terms of simulation/computation period, as stated previously. A final remark is that biomass gasification and/or devolatilization, as well as depletion and creation of tar, took a place in a very short period; as soon as the gasification and/or devolatilization process took place, the yields of gases, tar, and char achieved the steady state. When the gasification and/or devolatilization heating was low (<700 K), the gasification and/or devolatilization of micro-scale size biomass particles was almost null. From 700 to 900 K, gasification and/or devolatilization started and almost terminated for char and gases; however, at a temperature of 1050 K, gasification and/or devolatilization was fully completed and, in turn, there were no further gasification and/or devolatilization processes at higher temperatures (between 1050 and 1400 K). Analysis of mass loss of biomass powder showed that the total volatile yield (tar and gases) was about 85% in dry basis.

It should be pointed out that the kinetic rate constants used in the different mechanisms were different for different biomass sources and particle sizes as well as the heating conditions. In the present work, these parameters were calibrated using the data of Nunn et al. [50], which had fast heating conditions similar to the current flame. The numerical results from all models were in good agreement with the measured data. One may also notice that there were minor differences between the numerical simulation of the different models (M1, M2, and M3), as shown in Figures 3–5. In model 1 (M1), as shown in Figure 3, the mass loss rate of biomass was slow in the begging (from T = 400–700 K), whereas in model 2 (M2), it is a little faster (as shown in Figure 4); however, mass loss rate of model 3 (M3) came in between M1 and M2, as shown in Figure 5. In temperatures between 700 K and 900 K, the mass loss rates of biomass in M1 and M2 were underestimated, but M3 was overestimated, when compared with experimental data. Regarding the gas simulation, both M1 and M3 were almost identical, and they matched the experimental data; however, M2 was slightly overestimated. Regarding the tar simulation of different models, compared to the experimental data, as shown in Figures 3–5, tar in M3 was underestimated, M2 was overestimated, and M1 almost matched the experimental data. The char for all simulated models were almost identical, as shown in Figures 3–5.

5. Conclusions

Biomass is one of the largest renewable energy sources worldwide. Biomass in a powder form is an encouraging renewable source of energy because it burns like a gas. From such a view, biomass powder was investigated as a renewable form of fuel for internal combustion engines (ICEs). In the current study, modeling and validation of the biomass powder combustion in ICEs was carried out for first time. The modelling tools included particle tracing, drying, shrinkage, and gasification/devolatilization processes; furthermore, a number of new gasification/devolatilization models was proposed using parallel and/or series reaction scheme mechanisms, as the gasification/devolatilization process is one of the most important and probably the most complicated processes. During the gasification/devolatilization process, biomass powders were accelerated because of the fast moisture and gases released; such phenomenon would affect biomass powder distribution and, in turn, powder flame in combustion engines. The effect/phenomenon was modeled as well. During gasification/devolatilization of biomass powder, tar was formed and oxidized. The tar gasification and/or devolatilization model was included as well. Comparisons between numerical simulation, including all the mathematical models, and the experimental data were carried out, and results

showed good agreement. Results also showed that gasification/devolatilization models 1, 2, and 3 were capable of reproducing the mass yields of gases, tar, and char perfectly. Model 3 was somewhat simple and economical in the simulation/computation; however, models 1 and 2 were slightly computationally heavy.

References

1. Elfasakhany, A. Investigation on performance and emissions characteristics of an internal combustion engine fuelled with petroleum gasoline and a hybrid methanol-gasoline fuel. *Int. J. Eng. Technol.* **2013**, *13*, 24–43.

2. Elfasakhany, A. The Effects of Ethanol-Gasoline Blends on Performance and Exhaust Emission Characteristics of Spark Ignition Engines. *Int. J. Automot. Eng.* **2014**, *4*, 608–620.

3. Elfasakhany, A. Experimental study on emissions and performance of an internal combustion engine fueled with gasoline and gasoline/n-butanol blends. *Energy Convers. Manag.* **2014**, *88*, 277–283. [CrossRef]

4. Elfasakhany, A. Experimental investigation on SI engine using gasoline and a hybrid iso-butanol/gasoline fuel. *Energy Convers. Manag.* **2015**, *95*, 398–405. [CrossRef]

5. Elfasakhany, A. Investigations on the effects of ethanol-methanol-gasoline blends in a spark-ignition engine: Performance and emissions analysis. *Eng. Sci. Technol.* **2015**, *18*, 713–719. [CrossRef]

6. Elfasakhany, A. Experimental study of dual n-butanol and iso-butanol additives on spark-ignition engine performance and emissions. *Fuel* **2016**, *163*, 166–174. [CrossRef]

7. Elfasakhany, A. Performance and emissions analysis on using acetone–gasoline fuel blends in spark ignition engine. *Eng. Sci. Technol.* **2016**, *19*, 1224–1232. [CrossRef]

8. Elfasakhany, A.; Mahrous, A.-F. Performance and emissions assessment of n-butanol–methanol–gasoline blends as a fuel in spark-ignition engines. *Alex. Eng. J.* **2016**, *55*, 3015–3024. [CrossRef]

9. Elfasakhany, A. Engine performance evaluation and pollutant emissions analysis using ternary bio-ethanol–iso-butanol–gasoline blends in gasoline engines. *J. Clean. Prod.* **2016**, *139*, 1057–1067. [CrossRef]

10. Elfasakhany, A. Performance and emissions of spark-ignition engine using ethanol–methanol–gasoline, n-butanol–iso-butanol–gasoline and iso-butanol–ethanol–gasoline blends: A comparative study. *Eng. Sci. Technol.* **2016**, *19*, 2053–2059. [CrossRef]

11. Elfasakhany, A. Investigations on performance and pollutant emissions of spark-ignition engines fueled with n-butanol–, iso-butanol–, ethanol–, methanol–, and acetone–gasoline blends: A comparative study. *Renew. Sustain. Energy Rev.* **2017**, *71*, 404–413. [CrossRef]

12. Elfasakhany, A. Exhaust emissions and performance of ternary iso-butanol–bio-methanol–gasoline and n-butanol–bio-ethanol–gasoline fuel blends in spark-ignition engines: Assessment and comparison. *Energy* **2018**, *158*, 830–840. [CrossRef]

13. Elfasakhany, A. *Alcohols as Fuels in Spark Ignition Engines: Second Blended Generation*; Lambert Academic Publishing: Saarbrucken, Germany, 2017; ISBN 978-3-659-97691-9.

14. Elfasakhany, A. Biofuels in Automobiles: Advantages and Disadvantages: A Review. *Curr. Altern. Energy* **2019**, *3*, 1–7. [CrossRef]

15. Elfasakhany, A. *Benefits and Drawbacks on the Use Biofuels in Spark Ignition Engines*; Lambert Academic Publishing: Saarbrucken, Germany, 2017; ISBN 978-620-2-05720-2.

16. Elfasakhany, A.; Bai, X.S. *Simulation of Wood Powder Flames in a Vertical Furnace*, 3rd ed.; Combustion Symposium: Marrakech, Morocco, 2003; p. 144.

17. Elfasakhany, A.; Tao, L.X.; Bai, X.S. Transport of pulverized wood particles in turbulent flow: Numerical and experimental studies. *Energy Procedia* **2014**, *61*, 1540–1543. [CrossRef]

18. Vamvuka, D.; Karakas, E.; Kastanaki, E.; Grammelis, P. Pyrolysis characteristics and kinetics of biomass residuals mixtures with lignite. *Fuel* **2003**, *82*, 1949–1960. [CrossRef]

19. Elfasakhany, A. Modelling of Pulverised Wood Flames. Ph.D. Thesis, Lund Univ., Lund, Sweden, 2005.

20. Elfasakhany, A.; Bai, X.S. Numerical and experimental studies of irregular-shape biomass particle motions in turbulent flows. *Eng. Sci. Technol.* **2019**, *22*, 249–265. [CrossRef]

21. Elfasakhany, A.; Bai, X.S.; Espenas, B.; Tao, L.; Larfeldt, J. Effect of Moisture and Volatile Releases on Motion of Pulverised Wood Particles. In Proceedings of the 7th Int. Conf. on Energy for a Clean Environment, Lisbon, Portugal, 7–10 July 2003; p. 167.

22. Tao, L.; Berge, N.; Elfasakhany, A.; Bai, X.S. Experimental and Numerical Studies of a Pulverised Wood Flame. In Proceedings of the 6th European Conf. on Industrial Furnaces and Boilers, Lisbon, Portugal, 2–5 April 2002.

23. Elfasakhany, A.; Tao, L.; Espenas, B.; Larfeldt, J.; Bai, X.S. Pulverised Wood Combustion in a Vertical Furnace: Experimental and Computational Analyses. *Appl. Energy* **2013**, *112*, 454–464. [CrossRef]

24. Elfasakhany, A.; Bai, X.S. Modelling of pulverised wood combustion: A comparison of different models. *Prog. Comput. Fluid Dyn.* **2006**, *6*, 188–199. [CrossRef]

25. Sadhukhan, A.K.; Gupta, P.; Goyal, T.; Saha, R.K. Modelling of pyrolysis of coal–biomass blends using thermogravimetric analysis. *Bioresour. Technol.* **2008**, *99*, 8022–8026. [CrossRef] [PubMed]

26. Sepman, A.V.; de Goey, L.P.H. Plate reactor as an analysis tool for rapid pyrolysis of biomass. *Biomass Bioenergy* **2011**, *35*, 2903–2909. [CrossRef]

27. Kaushal, P.; Abedi, J.; Mahinpey, N. A comprehensive mathematical model for biomass gasification in a bubbling fluidized bed reactor. *Fuel* **2010**, *89*, 3650–3661. [CrossRef]

28. Hatakeyama, T.; Quinn, F.X. *Thermal Analysis—Fundamentals and Applications to Polymer Science*; John Wiley & Sons Ltd.: Hoboken, NJ, USA, 1999.

29. Haykiri-Acma, H.; Yaman, S. Synergy in devolatilization characteristics of lignite and hazelnut shell during co-pyrolysis. *Fuel* **2007**, *86*, 273–380. [CrossRef]

30. Meesri, C.; Moghtaderi, B. Lack of synergetic effects in the pyrolytic characteristics of woody biomass/coal blends under low and high heating rate regimes. *Biomass Bioenergy* **2002**, *23*, 55–66. [CrossRef]

31. Nassar, M.N. Thermal analysis of kinetics of Bagasse and Rice Straw. *Energy Sources* **1999**, *21*, 131–137. [CrossRef]

32. Vuthaluru, H.B. Investigation into the pyrolytic behaviour of coal/biomass blends using thermogravimetric analysis. *Bioresour. Technol.* **2004**, *92*, 187–195. [CrossRef]

33. Sutcu, H. Pyrolysis by thermogravimetric analysis of blends of peat with coals of different characteristics and biomass. *J. Chin. Inst. Chem. Eng.* **2007**, *38*, 245–249. [CrossRef]

34. Zhou, L.; Wang, Y.; Huang, Q.; Cai, J. Thermogravimetric characteristics and kinetics of plastic and biomass blends co-pyrolysis. *Fuel Process. Technol.* **2006**, *87*, 963–969. [CrossRef]

35. Di Blasi, C. Modelling chemical and physical processes of wood and biomass pyrolysis. *Prog. Energy Combust. Sci.* **2008**, *34*, 47–90. [CrossRef]

36. Rodrigo, C.R.L.; Manoel, F.M.N.; Danielle, R.S.G. CFD modeling of a small-scale cyclonic combustor chamber using biomass powder. *Energy Procedia* **2017**, *120*, 556–563. [CrossRef]

37. Fabio, C.L.; Stefano, C.; Alessandro, M.; Vincenzo, M. Vittorio Rocco. Analysis of Residual biomass Fast Pyrolysis at Laboratory Scale: Experimental and Numerical Evaluation of Spent Coffee powder Energy Content. *Energy Procedia* **2017**, *105*, 817–822.

38. Saad, A.; El-Sayed, M.E.M. Pyrolysis characteristics and kinetic parameters determination of biomass fuel powder by differential thermal gravimetric analysis (TGA/DTG). *Energy Convers. Manag.* **2014**, *85*, 2014.

39. Xu, G.; Li, M.; Lu, P. Experimental investigation on flow properties of different biomass and torrefied biomass powder. *Biomass Bioenergy* **2019**, *122*, 63–75. [CrossRef]

40. Pachón-Morales, J.; Colin, J.; Pierre, F.; Puel, F.; Perré, P. Effect of torrefaction intensity on the flow properties of lignocellulosic biomass powder. *Biomass Bioenergy* **2019**, *120*, 301–312. [CrossRef]

41. Pachón-Morales, J.; Huy, D.; Colin, J.; François, P.; Dingena, S. DEM modelling for flow of cohesive lignocellulosic biomass powders: Model calibration using bulk tests. *Adv. Powder Technol.* **2019**, *30*, 732–750. [CrossRef]

42. Li, M.; Li, Y.; Cai, Q.; Zhou, S. Spraying carbon powder derived from mango wood biomass as high-performance anode in bio-electrochemical system. *Bioresour. Technol.* **2020**, *300*, 122623. [CrossRef] [PubMed]

43. Medina, C.H.; Phylaktou, H.N.; Sattar, H.; Andrews, G.E.; Gibbs, B.M. The development of an experimental method for the determination of the minimum explosible concentration of biomass powder. *Biomass Bioenergy* **2013**, *53*, 95–104. [CrossRef]

44. Joel, F.; Robert, J.; Markus, B.; Sylvia, H.L. Mass flow and variability in screw feeding of biomass powder—Relations to particle and bulk properties. *Powder Technol.* **2015**, *276*, 80–88.

45. He, F.; Yi, W.; Li, Y.; Zha, J.; Luo, B. Effects of fuel properties on the natural downward smoldering of piled biomass powder: Experimental investigation. *Biomass Bioenergy* **2014**, *67*, 288–296. [CrossRef]

46. Xie, T.; Wei, R.; Wang, Z.; Wang, J. Comparative analysis of thermal oxidative decomposition and fire characteristics for different straw powder via thermogravimetry and cone calorimetry. *Process Saf. Environ. Prot.* **2020**, *134*, 121–130. [CrossRef]

47. Bridgwater, A.V.; Peacock, G.V.C. Fast pyrolysis processes for biomass. *Renew. Sustain. Energy Rev.* **2000**, *4*, 1–73. [CrossRef]

48. Goyal, H.B.; Seal, D.; Saxena, R.C. Bio-fuels from thermochemical conversion of renewable resources: A review. *Renew. Sustain. Energy Rev.* **2008**, *12*, 504–517. [CrossRef]

49. Elfasakhany, A. Powder biomass fast pyrolysis as in combustion conditions: Numerical prediction and validation. *Renew. Energy Focus* **2018**, *27*, 78–87. [CrossRef]

50. Howard, T.R.N.J.; Longwell, J.; Peters, W. Product compositions and kinetics in the rapid pyrolysis of sweet gum hardwood. *Ind. Eng. Chem. Proc. Des. Dev.* **1985**, *24*, 836–844.

51. Rusaas, J. Numerical Simulation of Gas-Particle Flow Linked to Pulverised Coal Combustion. Ph.D. Thesis, Institute of Energy Technology, Aalborg University, Aalborg, Denmark, 1998.

52. Ganser, G.H. A rational approach to drag prediction of spherical and nonspherical particles. *Powder Technol.* **1993**, *77*, 143–152. [CrossRef]

53. Chhabra, R.P.; Agarwal, L.; Sinha, N.K. Drag on non-spherical particles: An evaluation of available methods. *Powder Technol.* **1999**, *101*, 288–295. [CrossRef]

54. Shin, D.; Choi, S. The combustion of simulated waste particle in a fixed bed. *Combust. Flame* **2020**, *121*, 167–180. [CrossRef]

55. Bryden, K.M.; Ragland, K.W.; Rutland, C.J. Modeling thermally thick pyrolysis of wood. *Biomass Bioenergy* **2002**, *22*, 41–53. [CrossRef]

56. Hasanah, U.; Setiaji, B.; Anwar, C. The Chemical Composition and Physical Properties of the Light and Heavy Tar Resulted from Coconut Shell Pyrolysis. *J. Pure Appl. Chem. Res.* **2012**, *1*, 26–32. [CrossRef]

57. Elfasakhany, A. Modelling of Secondary Reactions of Tar (SRT) Using a Functional Group Model. *Int. J. Mech. Eng. Tech.* **2012**, *3*, 123–136.

58. Magnussen, B.; Hjertager, B. On mathematical modelling of turbulent combustion with special emphasis on soot formation and combustion. *Proc. Combust. Inst.* **1976**, *16*, 719–729. [CrossRef]

59. Larfeldt, J.; Leckner, B.; Melaaen, M.C. Modeling and measurements of the pyrolysis of large wood particles. *Fuel* **2000**, *79*, 1637–1643. [CrossRef]

60. Di Blasi, C. Heat, momentum and mass transfer through a shrinkage biomass particle exposed to thermal radiation. *Chem. Eng. Sci.* **1996**, *51*, 1121–1132. [CrossRef]

61. Kops, S.M.B.; Malte, P.C. *Simulation and Modelling of Wood Dust Combustion in Cyclone Burners—Final Technical Report*; U.S. Department of Energy: Washington, DC, USA, 2004.

62. Felipe, R.C.; Rogério, B.; Francis, H.R.F.; Cristiano, V.S. Application of the WSGG model for the calculation of gas–soot radiation in a turbulent non-premixed methane–air flame inside a cylindrical combustion chamber. *Int. J. Heat Mass Transf.* **2016**, *93*, 742–753.

63. Elfasakhany, A.; Klason, T.; Bai, X.S. Modelling of pulverised wood combustion using a functional group model. *Combust. Theory Model.* **2008**, *12*, 883–904. [CrossRef]